

## Soil characterization for shallow landslides modeling: a case study in the Northern Apennines (Central Italy)

**Abstract** In this paper, we present preliminary results of the IPL project No. 198 “Multi-scale rainfall triggering models for Early Warning of Landslides (MUSE).” In particular, we perform an assessment of the geotechnical and hydrological parameters affecting the occurrence of landslides. The aim of this study is to improve the reliability of a physically based model high resolution slope stability simulator (HIRESSES) for the forecasting of shallow landslides. The model and the soil characterization have been tested in Northern Tuscany (Italy), along the Apennine chain, an area that is historically affected by shallow landslides. In this area, the main geotechnical and hydrological parameters controlling the shear strength and permeability of soils have been determined by in situ measurements integrated by laboratory analyses. Soil properties have been statistically characterized to provide more refined input data for the slope stability model. Finally, we have tested the ability of the model to predict the occurrence of shallow landslides in response to an intense meteoric precipitation.

**Keywords** Shallow landslides · Soil geotechnics · In situ measurements · Physically-based models · Instability mechanism triggering

### Introduction

Physically based approaches for modeling rainfall-induced shallow landslides are an intensely debated research topic among the earth sciences community, and many models have been presented thus far (Dietrich and Montgomery 1998; Simoni et al. 2008; Pack et al. 2001; Baum et al. 2002, 2010; Rossi et al. 2013; Lu and Godt 2008; Ren et al. 2010; Arnone et al. 2011). However, the application of models over large areas is hindered by a poor comprehension of the spatial organization of the required geotechnical and hydrological input parameters. The performance of a model can be strongly influenced by the errors or uncertainties in the input parameters (Segoni et al. 2009; Jiang et al. 2013).

In recent years, spatially variable soil thickness maps have frequently been incorporated in distributed slope stability modeling (Segoni et al. 2009; Jia et al. 2012; Mercogliano et al. 2013), but geotechnical and hydrological parameters have been proven to be more troublesome to manage because they are characterized by an inherent variability and their measurement is difficult, time-consuming, and expensive, especially when data are needed for large areas (Carrara et al. 2008; Baroni et al. 2010; Park et al. 2013).

As a consequence, in reviewing the literature about feeding distributed slope stability modeling with spatially variable geotechnical parameters, it is impossible to find an approach that is universally accepted and that can be used as a standard.

In many cases, for each geotechnical parameter, a constant value is used for the whole study area as averaged from in situ measurements (Jia et al. 2012) or derived from literature data. In some studies, a limited degree of spatial variability is ensured using a certain value for distinct

geological, lithological, or engineering geological units, as derived from direct measurements (Segoni et al. 2009; Baum et al. 2010; Montrasio et al. 2011; Zizioli et al. 2013) or from existing databases and published data (Lepore et al. 2013; Ren et al. 2014; Tao and Barros 2014).

The variability and uncertainty in geotechnical input parameters heavily reflect on the results when a deterministic approach is used in physically based models, and in recent years, the use of probabilistic approaches has widely increased as it allows a more proper consideration of uncertainties and inherent variability of the input data (Park et al. 2013). For instance, Santoso et al. (2011) used a probabilistic approach, even if limited to the characterization of the permeability, while many authors considered cohesion and friction angle as random variables using a probabilistic or stochastic approach (Park et al. 2013; Griffiths et al. 2011; Chen and Zhang 2014; Mercogliano et al. 2013)

The present work moves from this state of the art, and it shows a regional scale application of a distributed slope stability model. The study area (3103 km<sup>2</sup>) is located in Northern Tuscany (Italy), and the physically based distributed stability model used is developed by Rossi et al. (2013). In the area selected, the main geotechnical and hydrological parameters controlling the shear strength and permeability of soils have been determined by in situ measurements integrated with laboratory analyses. The data obtained have been studied in order to assess the relationships existing among the different parameters and the bedrock lithology. Soil properties have been then statistically characterized in order to define the input parameters in the physical model, with the final aim of testing the ability of the model to predict shallow landslide occurrence in response of an intense meteoric precipitation.

### Materials and methods

#### Description of the study area

The test area is located in Tuscany (North-central Italy) including a part of the Northern Apennines mountains chain, with an extension of 3103 km<sup>2</sup> (Fig. 1).

The Northern Apennines is a complex thrust-belt system made up of the juxtaposition of several tectonic units, piled during the Tertiary under a compressive regime that was followed by extensional tectonics from the Upper Tortonian (Vai and Martini 2001). This phase produced a sequence of horst-graben structures with an alignment NW-SE that resulted in the emplacement of Neogene sedimentary basins, mainly of marine (to the West) and fluvio-lacustrine (to the East) origin. Today, the morphology is dictated by the presence of NW-SE trending ridges where Mesozoic and Tertiary flysch and calcareous units outcrop, separated by Pliocene-Quaternary basins. The intermountain basins were formed from the Upper Tortonian (in the South-West) to the Upper Pliocene and Pleistocene (in the North-East). While the first ones experienced several episodes of marine regression and transgression during the Miocene and Pliocene, the second ones were characterized by a fluvio-lacustrine depositional environment.

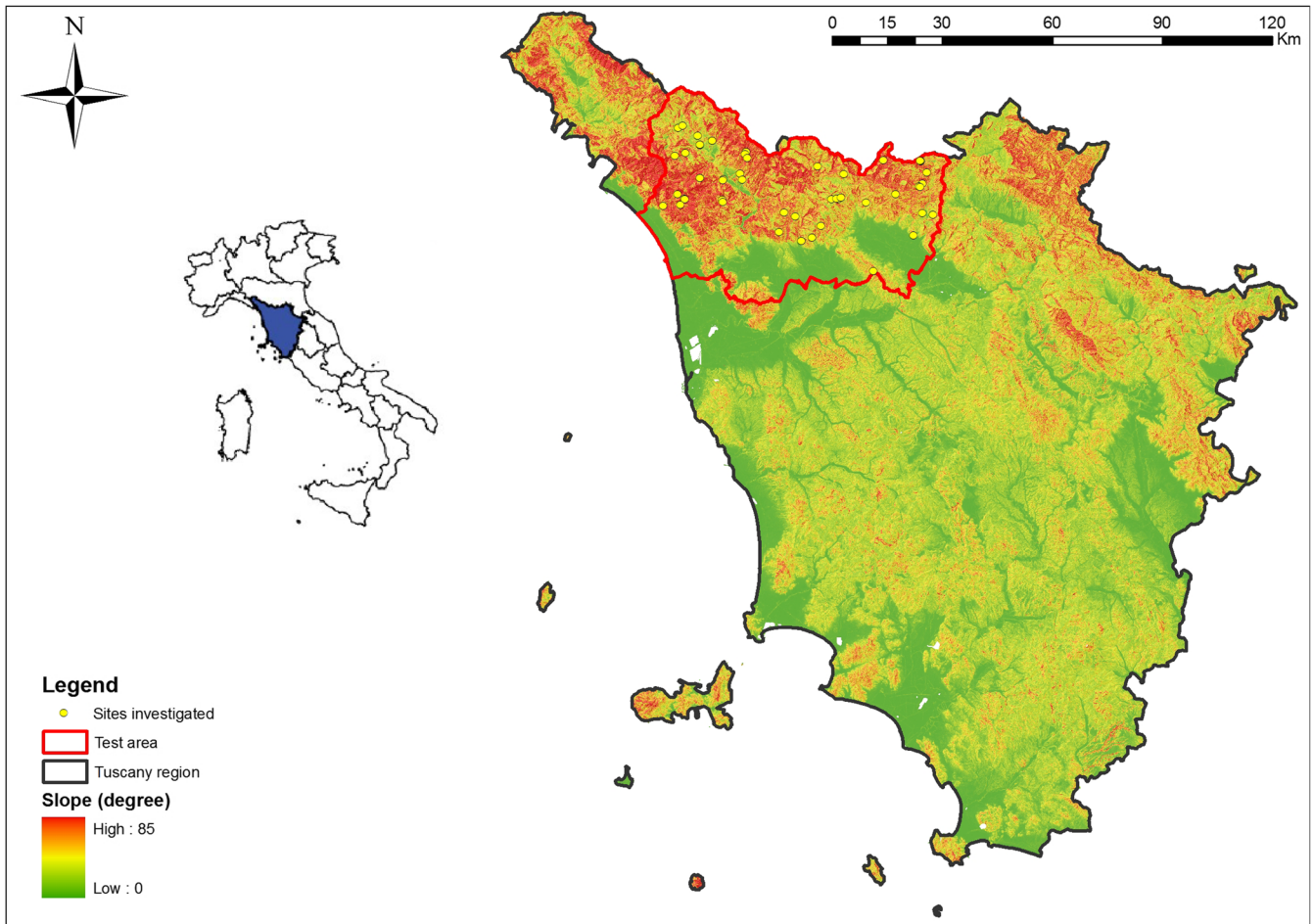


Fig. 1 Study area

These geological settings clearly affect the typology and occurrence of surface processes, primarily through the differences in the mechanical properties related to the various prevalent lithologies. The study area, which includes the provinces of Pistoia, Prato e Lucca, shows two different geological settings in the east and west sectors, respectively.

In the western sector, the ridges that divide the basins are usually made up of carbonaceous rocks with slope gradients greater than  $60^\circ$ , often subvertical or vertical. These slopes are usually rocky, with discontinuous vegetation and without the presence of forests. Moving downslope, the metamorphic sandstone and phyllitic-schists substitute carbonaceous rocks, with the bedrock usually covered by talus and scree deposits. In this case, slopes are usually moderately steep (values ranging from  $25^\circ$  to  $40^\circ$ ) and are largely characterized by soils that developed from a predominantly phyllitic-schist and metamorphic-arenaceous bedrock, mantled by dense forest (mainly chestnut). On the contrary, the calcareous and dolomitic slopes are usually rocky or with very thin soil cover. The soils covering metamorphic sandstone and phyllite are usually the most involved in landsliding; these soils are rather thin (0.5–2 m thick).

The eastern sector shows a more uniform geological condition with the prevalence of flysch formation rock-type (Macigno), which is composed of quartz and feldspar sandstone alternated with layers of siltstone. Slope gradients are generally lower than in the western sector,

with maximum values up to  $55^\circ$ . In the mid and upper sections of the valley, where most of the landslides usually occur, the stratigraphy consists of a 1.5 to 5 m thick layer of colluvial soil overlying the bedrock.

A new lithological classification of the study area has been carried out utilizing the Regional Geological Map at the scale of 1:10,000 (Fig. 2). Six lithological classes have been defined according to Catani et al. (2005), and each geological formation has been attributed to one lithological class, based on the predominant lithology. At this scope, 68 geological maps have been used and 194 geological formations have been classified according to the classification scheme adopted. The six lithologies defined are cohesive and granular soils, hard rocks, marls and compact clays, weakly cemented conglomerates and loose carbonates rocks, rocks with pelitic layers, and complex mainly pelitic units.

Figure 2 shows the newly derived lithological map of the area. In the southern portion, mainly flat areas, cohesive and granular soils outcrop. In the eastern sector, there is the predominance of flysch units, mainly complex units with predominance of sandstone with pelitic layers and complex units with predominance of argillaceous material. In the western sector, hard rocks, mainly phyllitic-schist and metamorphic-arenaceous rocks predominate shales, limestones, and conglomerates.

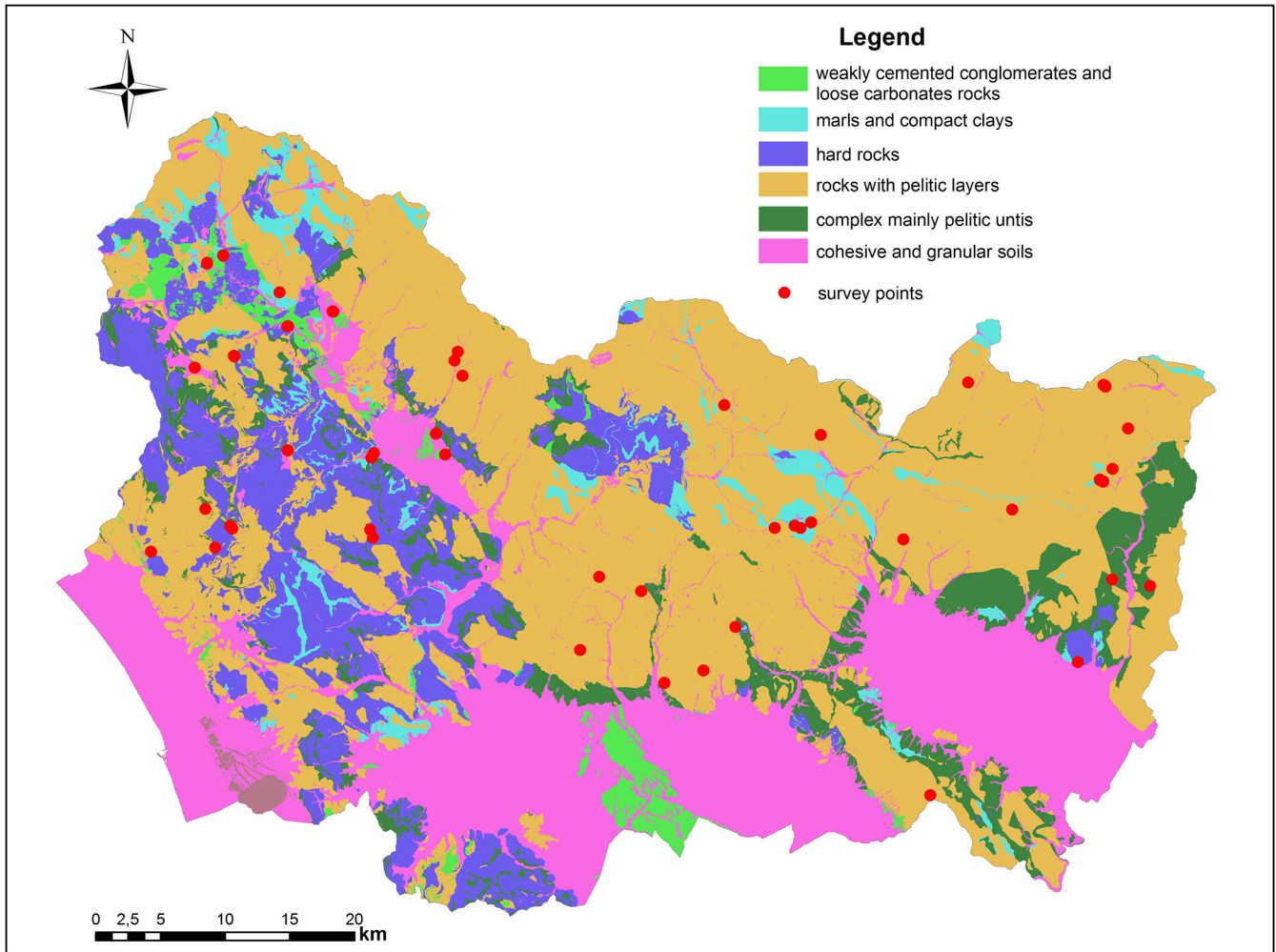


**Fig. 2** Lithological map and survey points

### Laboratory and in situ measurements

A complete geotechnical characterization campaign of the soil cover has been carried out in the study area. The survey points have been selected in order to have a homogenous distribution (Fig. 2) for all the lithologies shown in Fig. 2. The soils have been sampled at depths ranging from 0.4 to 0.8 m b.g.l. (below the ground level) (Table 1). The depth of the soil samples can be considered significant to characterize the soil material involved in landsliding. As pointed out in Giannecchini (2006), Giannecchini et al. (2007), D'Amato Avanzi et al. (2009), and D'Amato Avanzi et al. (2013), the depth of the sliding surface of shallow landslides that usually occur in the study area is around 1 m deep.

The geotechnical parameters of soils were determined by a series of in situ and laboratory tests. Field tests are more difficult to manage and control than laboratory tests, but they are considered to give a more direct and representative measurement of the real in situ soil properties (Baroni et al. 2010). The in situ tests included the Borehole Shear Test (BST; Lutenegeger and Halberg 1981), which provides the shear strength parameters under natural conditions without disturbing the soil samples, matric suction measurements with a tensiometer, and a constant head permeameter test performed with an Amoozegar

(1989). Additionally, a series of laboratory tests was conducted, including the determination of grain size distribution, the Atterberg limits, and the phase relationship analysis.

The BST test was performed on soils in unsaturated conditions, meaning that they are subjected to pore water pressure ( $u_w$ ) conditions lower than that of air pressures ( $u_a$ ). At the same depth as the BST, matric suction values ( $u_a - u_w$ ) were measured with tensiometers. The interpretation of the BST results were made using the Fredlund et al. (1978) slope failure equation for unsaturated soils as suggested by Rinaldi and Casagli (1999), Casagli et al. (2006), and Tofani et al. (2006):

$$\tau = c' + (\sigma - u_a)\tan\phi' + (u_a - u_w)\tan\phi^b \quad (1)$$

where  $\tau$  is the shear strength,  $c'$  is the effective cohesion,  $\sigma$  is the total normal stress,  $u_a$  is the pore air pressure due to surface tension,  $\phi'$  is the effective friction angle,  $u_w$  is the pore water pressure, and  $\phi^b$  is the angle expressing the rate of strength increase related to matric suction. BSTs were performed within an interval of  $\sigma$  values of 20–80 kPa. Effective cohesion is measured by means of direct shear tests, which have been carried out

**Table 1** Geotechnical properties of the 59 sites investigated

Site name	Bedrock lithology	UTM-E (m)	UTM-N (m)	BST depth (m)	$\phi'$ (°) BST	c (kPa) BST	$\phi'$ (°) DT	Matric suction (kPa)	Gravel (%)	Sand (%)
Filecchio	Conglomerates and poorly cemented rocks	620,408	4,879,260	0.6	28	7	n.a.	48.8	6.8	31.9
Galliano 1	Conglomerates and poorly cemented rocks	615,149	4,879,370	0.6	30	2	n.a.	58.3	11.2	35.1
Galliano 2	Conglomerates and poorly cemented rocks	614,974	4,879,027	0.6	23	5	n.a.	50.2	11.2	35.1
San Michele 1	Conglomerates and poorly cemented rocks	602,871	4,893,347	0.6	28	14	n.a.	36.5	6.0	29.8
San Michele 2	Conglomerates and poorly cemented rocks	602,882	4,893,397	0.6	34	3	n.a.	49.4	4.8	29.7
Buvicchia 1	Cohesive and granular soils	619,730	4,880,813	0.6	36	3	n.a.	35.1	7.4	56.5
Buvicchia 2	Cohesive and granular soils	619,767	4,880,815	0.6	n.a.	0	n.a.	40.3	n.a.	n.a.
Cerreta 1	Cohesive and granular soils	608,816	4,879,581	n.a.	32	n.a.	n.a.	n.a.	40.2	38.1
Cerreta 2	Cohesive and granular soils	608,816	4,879,580	n.a.	37	n.a.	n.a.	n.a.	57.9	27.6
Cerreta 3	Cohesive and granular soils	608,816	4,879,580	n.a.	38	n.a.	n.a.	n.a.	34.4	49.0
Fontana delle Monache	Cohesive and granular soils	601,973	4,885,684	0.6	n.a.	10	n.a.	62.5	12.4	14.1
Mandola 1	Cohesive and granular soils	604,062	4,893,959	0.5	27	1	n.a.	50.8	33.3	19.9
Soffiana 1	Cohesive and granular soils	612,139	4,889,809	0.6	33	3	n.a.	68.5	0.4	3.7
Soffiana 2	Cohesive and granular soils	612,167	4,889,785	0.6	35	1	n.a.	50.8	1.2	9.6
Termini 2	Cohesive and granular soils	608,842	4,888,715	0.6	33	10	n.a.	38.9	10.4	74.4
Savignano	Complex mainly pelitic units	672,328	4,869,578	0.6	n.a.	9	n.a.	79.9	34.0	40.5
Schignano	Complex mainly pelitic units	669,523	4,870,061	0.5	n.a.	13	n.a.	90.4	19.4	36.3
Galcei	Hard rocks	666,997	4,863,985	n.a.	n.a.	n.a.	n.a.	n.a.	19.5	45.2
Termini 1	Hard rocks	608,792	4,888,705	0.5	30	12	n.a.	39.3	11.4	74.9
Vallico sopra-Vallico Sotto 1	Hard rocks	614,901	4,873,730	0.6	37	11	n.a.	40.5	23.9	29.7
Vallico sopra-Vallico Sotto 2	Hard rocks	615,085	4,873,155	0.6	30	4	n.a.	39.8	24.1	27.5
Poggiolino 1	Marls and compact clays	646,141	4,874,037	0.5	n.a.	1	n.a.	15.0	15.9	18.0
Luicciana Marne	Marls and compact clays	668,862	4,877,273	n.a.	38	n.a.	n.a.	n.a.	23.3	37.9
Mandola 2	Marls and compact clays	604,080	4,893,925	0.6	36	12	n.a.	65.8	31.5	23.7
Poggiolino 2	Marls and compact clays	646,571	4,873,865	0.5	31	0	n.a.	68.3	37.3	34.6



Table 1 (continued)

Site name	Bedrock lithology	UTM-E (m)	UTM-N (m)	BST depth (m)	$\phi'$ ( $^{\circ}$ ) BST	c (kPa) BST	$\phi'$ ( $^{\circ}$ ) DT	Matric suction (kPa)	Gravel (%)	Sand (%)
Risvolta 1	Marls and compact clays	669,560	4,878,201	0.6	34	7	n.a.	34.0	22.7	45.8
Acquerino	Rocks with pelitic layers	662,151	4,875,219	0.5	33	2	n.a.	10.0	26.7	43.6
Barga 1	Rocks with pelitic layers	621,342	4,886,844	n.a.	37	n.a.	n.a.	n.a.	17.1	64.0
Barga 2	Rocks with pelitic layers	621,109	4,886,196	n.a.	35	n.a.	n.a.	n.a.	7.5	66.5
Barga 3	Rocks with pelitic layers	621,691	4,885,080	n.a.	37	n.a.	n.a.	n.a.	13.0	66.2
Boveglio	Rocks with pelitic layers	631,747	4,870,254	0.5	33	4	n.a.	3.2	50.9	26.0
Corbezi	Rocks with pelitic layers	654,144	4,873,020	0.4	20	1	n.a.	74.7	38.1	32.6
Foresta del Teso	Rocks with pelitic layers	648,075	4,880,713	0.5	34	2	n.a.	58.5	16.1	54.9
Gove	Rocks with pelitic layers	641,781	4,866,585	n.a.	30	n.a.	n.a.	n.a.	7.7	56.2
Le Piastre	Rocks with pelitic layers	647,364	4,874,283	0.6	42	3	n.a.	21.8	33.6	31.0
Levigliani	Rocks with pelitic layers	602,747	4,875,262	0.6	36	8	28	14.0	30.5	21.6
Lizzano	Rocks with pelitic layers	640,968	4,882,912	0.5	34	6	n.a.	8.4	27.6	41.0
Luicciana Arenarie	Rocks with pelitic layers	668,618	4,877,418	0.6	34	12	n.a.	20.6	30.0	20.2
Marcaccio	Rocks with pelitic layers	598,747	4,872,110	0.6	n.a.	7	n.a.	57.9	18.2	10.5
Massa e Cozzile 1	Rocks with pelitic layers	639,426	4,863,363	0.5	31	4	29	7.2	0.8	85.4
Massa e Cozzile 2	Rocks with pelitic layers	639,426	4,863,360	0.7	39	4	n.a.	7.2	n.a.	n.a.
Molino di Gufinaia	Rocks with pelitic layers	670,707	4,881,186	0.6	33	1	n.a.	42.0	6.6	27.2
Pizzorne	Rocks with pelitic layers	630,351	4,864,882	0.6	30	1	n.a.	3.0	10.3	39.1
Poggio di Petto 1	Rocks with pelitic layers	668,891	4,884,411	0.7	36	19	n.a.	80.3	27.5	35.3
Poggio di Petto 2	Rocks with pelitic layers	669,039	4,884,279	0.5	37	13	n.a.	77.1	9.1	16.9
Poggio di Petto 3	Rocks with pelitic layers	668,954	4,884,391	0.7	22	13	n.a.	34.0	n.a.	n.a.
Poggio di Petto 4	Rocks with pelitic layers	668,992	4,884,351	0.7	21	2	n.a.	12.1	n.a.	n.a.
Porciano	Rocks with pelitic layers	656,141	4,854,170	0.4	31	n.a.	n.a.	n.a.	30.7	54.5
Posola	Rocks with pelitic layers	658,912	4,884,582	0.4	41	0	n.a.	7.0	31.9	25.9
Prunetta	Rocks with pelitic layers	644,682	4,873,872	0.4	31	0	n.a.	74.5	11.1	76.0
Pruno-Volegno 1	Rocks with pelitic layers	604,730	4,873,817	n.a.	23	n.a.	29	n.a.	21.5	38.7
Pruno-Volegno 2	Rocks with pelitic layers	604,591	4,874,022	0.5	n.a.	6	n.a.	6.0	14.9	34.0
Rifugio Uso di Sotto	Rocks with pelitic layers	634,835	4,869,192	0.5	n.a.	0	n.a.	4.8	33.2	43.3
Risvolta 2	Rocks with pelitic layers	603,481	4,872,409	0.5	n.a.	7	n.a.	32.3	19.1	10.7
Sillicagnano	Rocks with pelitic layers	608,215	4,891,224	0.5	29	1	n.a.	34.7	0.2	61.9

ICL/IPL Activities

Table 1 (continued)

Site name	Bedrock lithology	UTM-E (m)	UTM-N (m)	BST depth (m)	$\phi'$ (°) BST	c (kPa) BST	$\phi'$ (°) DT	Matric suction (kPa)	Gravel (%)	Sand (%)
Uzzano 1	Rocks with pelitic layers	636,557	4,862,445	0.5	38	6	33	3.0	12.1	43.1
Uzzano 2	Rocks with pelitic layers	636,556	4,862,443	0.8	26	6	n.a.	3.0	7.0	47.8
Vergaia 1	Rocks with pelitic layers	604,851	4,886,543	0.6	32	2	n.a.	58.5	4.1	60.5
Vergaia 2	Rocks with pelitic layers	604,898	4,886,509	0.5	23	3	n.a.	38.0	9.6	51.3
Site name	Silt (%)	Clay (%)	USCS	$W_r$ (%)	$W_L$ (%)	$W_p$ (%)	IP (%)	$\gamma$ (kN/m <sup>3</sup> )	$\gamma_d$ (kN/m <sup>3</sup> )	Bulk porosity <i>n</i> (%)
Filecchio	46.7	14.6	CL	5.0	36	23	13	12.0	11.5	55.9
Galicano 1	41.1	12.6	ML	4.1	42	32	10	n.a.	n.a.	n.a.
Galicano 2	41.1	12.6	OL	26.8	41	34	7	n.a.	n.a.	n.a.
San Michele 1	42.4	21.8	OL	24.9	42	39	3	n.a.	n.a.	n.a.
San Michele 2	46.3	19.2	ML	n.a.	37	35	2	n.a.	n.a.	n.a.
Buvicchia 1	32.0	4.1	ML	15.9	34	32	2	12.1	10.4	n.a.
Buvicchia 2	n.a.	n.a.	n.a.	n.a.	36	32	4	n.a.	n.a.	n.a.
Cerreta 1	18.5	3.2	n.a.	18.5	n.a.	n.a.	n.a.	12.8	10.8	n.a.
Cerreta 2	12.6	1.9	n.a.	15.2	n.a.	n.a.	n.a.	13.4	11.6	55.3
Cerreta 3	12.5	4.1	SM	14.8	n.a.	n.a.	n.a.	14.1	12.3	52.8
Fontana delle Monache	58.4	15.1	MH	23.5	58	34	24	n.a.	n.a.	n.a.
Mandola 1	31.0	15.8	CL	16.2	25	11	14	n.a.	n.a.	n.a.
Soffiana 1	53.1	42.8	ML	20.0	48	30	18	n.a.	n.a.	n.a.
Soffiana 2	51.3	37.9	CH	13.4	55	25	30	14.8	13.1	49.8
Termini 2	14.4	0.8	SM-SC	16.2	26	21	5	n.a.	n.a.	n.a.
Savignano	17.2	8.3	SM	9.9	n.a.	n.a.	n.a.	n.a.	n.a.	n.a.
Schignano	34.7	9.6	SM	13.9	n.a.	n.a.	n.a.	18.4	16.2	37.9
Galcei	25.2	10.1	SM	14.5	51	37	14	20.5	19.2	n.a.
Termini 1	12.8	0.9	SM-SC	n.a.	26	20	6	n.a.	n.a.	n.a.
Vallico sopra-Vallico Sotto 1	37.7	8.7	CH	43.5	57	28	29	n.a.	n.a.	n.a.
Vallico sopra-Vallico Sotto 2	37.5	10.9	CH	43.5	54	30	24	n.a.	n.a.	n.a.
Poggiolino 1	44.0	22.1	CL	22.4	36	23	13	19.3	15.8	39.2
Luiciana Mame	31.0	7.8	SM	16.9	36	31	5	n.a.	n.a.	n.a.
Mandola 2	27.9	16.9	CL	16.2	26	16	10	n.a.	n.a.	n.a.
Poggiolino 2	19.0	9.1	SC	9.6	35	17	18	23.3	21.3	18.2

**Table 1** (continued)

Site name	Silt (%)	Clay (%)	USCS	$W_r$ (%)	$W_L$ (%)	$W_P$ (%)	IP (%)	$\gamma$ (kN/m <sup>3</sup> )	$\gamma_d$ (kN/m <sup>3</sup> )	Bulk porosity $n$ (%)
Risvolta 1	24.1	7.4	SM	14.9	32	25	7	14,4	12,5	51,8
Acquerino	26.5	3.2	SM	31.5	35	24	11	18,0	13,7	47,3
Barga 1	17.5	1.4	SM	20.5	n.a.	n.a.	n.a.	13,9	11,5	55,6
Barga 2	25.5	0.5	SM	6.9	n.a.	n.a.	n.a.	19,5	18,3	n.a.
Barga 3	18.6	2.2	SM	26.5	n.a.	n.a.	n.a.	21,9	19,4	n.a.
Boveglio	18.5	4.6	GW	30.4	n.a.	n.a.	n.a.	19,6	15,0	42,2
Corbezzoli	25.8	3.5	SM	12.8	n.a.	n.a.	n.a.	14,8	13,1	49,5
Foresta del Teso	26.3	2.7	SM	11.7	n.a.	n.a.	n.a.	n.a.	n.a.	n.a.
Gove	29.6	6.5	SM	4.3	23	20	3	n.a.	n.a.	n.a.
Le Piastre	31.8	3.6	SM	19.8	35	30	5	20,6	17,2	33,8
Levigliani	45.2	2.7	ML	26.0	41	26	15	18,2	14,5	44,4
Lizzano	25.6	5.8	SM-SC	25.7	28	22	6	20,4	16,2	37,6
Luicciana Arenarie	29.7	20.1	ML	20.8	34	30	4	n.a.	n.a.	n.a.
Marcaccio	45.6	25.7	CH	43.5	57	24	33	n.a.	n.a.	n.a.
Massa e Cozzile 1	13.1	0.7	SM	n.a.	29	n.a.	n.a.	18,1	n.a.	n.a.
Massa e Cozzile 2	n.a.	n.a.	n.a.	n.a.	n.a.	n.a.	n.a.	n.a.	n.a.	n.a.
Molino di Guфинаia	42.0	24.2	ML-CL	18.0	28	21	7	n.a.	n.a.	n.a.
Pizzome	35.9	14.7	ML	35.3	36	30	7	17,2	12,7	51,1
Poggio di Petto 1	29.4	7.8	SM	13.6	31	24	7	n.a.	n.a.	n.a.
Poggio di Petto 2	56.7	17.3	ML	13.7	42	34	8	12,9	11,4	56,3
Poggio di Petto 3	n.a.	n.a.	n.a.	n.a.	n.a.	n.a.	n.a.	n.a.	n.a.	n.a.
Poggio di Petto 4	n.a.	n.a.	n.a.	n.a.	n.a.	n.a.	n.a.	n.a.	n.a.	n.a.
Porciano	14.0	0.8	SM	15.9	n.a.	n.a.	n.a.	n.a.	n.a.	n.a.
Posola	34.5	7.7	SM	26.4	30	25	5	18,1	14,3	44,9
Prunetta	9.1	3.8	SM	20.6	n.a.	n.a.	n.a.	n.a.	n.a.	n.a.
Pruno-Volegno 1	35.8	4.0	SM	30.0	32	21	11	17,2	13,3	49,0
Pruno-Volegno 2	44.9	6.2	CL	29.0	34	22	12	18,0	14,0	46,3
Rifugio Uso di Sotto	20.8	2.7	SM	27.5	31	24	7	19,4	15,2	41,5
Risvolta 2	52.8	17.4	CH	23.5	57	27	30	n.a.	n.a.	n.a.
Sillicagnano	34.8	3.1	SM	n.a.	51	37	14	n.a.	n.a.	n.a.
Uzzano 1	32.9	11.9	SC	21.2	26	16	10	19,3	15,9	38,7

Table 1 (continued)

Site name	Silt (%)	Clay (%)	USCS	$W_n$ (%)	$W_L$ (%)	$W_p$ (%)	IP (%)	$\gamma$ (kN/m <sup>3</sup> )	$\gamma_d$ (kN/m <sup>3</sup> )	Bulk porosity $n$ (%)
Uzzano 2	36.4	8.8	SM-SC	21.2	24	20	4	n.a.	n.a.	n.a.
Vergaia 1	25.6	9.8	SM-SC	16.2	26	21	5	n.a.	n.a.	n.a.
Vergaia 2	28.3	10.8	SC	16.2	26	14	12	n.a.	n.a.	n.a.

BS<sub>T</sub> borehole shear test, DT direct shear test, n.a. not available

only for few samples of the study area. However, the BST test was performed at shallow depths on mostly granular, normal consolidated materials, so that  $c'$  could be reasonably assumed to be equal to 0 kPa.

In Eq. (1), given a matric suction value, the horizontal projection of the failure envelope onto the plane  $\tau - (\sigma - u_a)$  represents a line with the following equation:

$$\tau = c + (\sigma - u_a)\tan\phi' \tag{2}$$

where the intercept is the total cohesion  $c$ . This results from the sum of the effective cohesion  $c'$  and the apparent cohesion due to the effects of matric suction (Casagli et al. 2006):

$$c = c' + (u_a - u_w)\tan\phi^b \tag{3}$$

The saturated hydraulic conductivity ( $k_s$ ) is one of the most difficult soil properties to measure, because of its marked temporal and spatial variability (Mallants et al. 1997; Warrick and Nielsen 1980) and because no benchmark standard measurement method has been established yet (Dirksen 1999; McKenzie and Cresswell 2008). The value of  $k_s$  within the unsaturated zone was measured in situ by using the Amoozemeter or Compact Constant Head Permeameter (CCHP). The procedure used for measuring  $k_s$  in the field is termed constant-head well permeameter technique (Philip 1985). Results are then entered into the Glover solution, which computes the saturated permeability of the soils:

$$k_s = \frac{Q \left[ \sinh^{-1} \left( \frac{h}{r} \right) - \left( \frac{r^2}{h^2} + 1 \right)^{\frac{1}{2}} + \frac{r}{h} \right]}{2\pi h^2} \tag{4}$$

where  $Q$  is the steady-state rate of water flow from the permeameter into the auger hole,  $\sinh^{-1}$  is the inverse hyperbolic sine function,  $h$  is the depth of water in the borehole (constant), and  $r$  is the radius of the borehole.

In addition to the in situ measures, the grain size distribution, the phase relationships (porosity, dry unit weight  $\gamma_d$ ), and the Atterberg limits are determined in the laboratory following the ASTM standards.

**HIRESSS description**

high resolution slope stability simulator (HIRESSS) (Rossi et al. 2013) is a physically based distributed slope stability simulator for analyzing shallow landslides triggering in real time, on large areas. The physical model is composed of two parts, hydrological and geotechnical. The hydrological one receives the rainfall data as dynamical input and computes the pressure head as perturbation to the geotechnical stability model, which provides results in terms of factor of safety ( $F_s$ ).

The hydrological model is based on an analytical solution of an approximated form of Richards equation under the wet condition hypothesis, and it is introduced as a modeled form of hydraulic diffusivity to improve the hydrological response. The geotechnical stability model is based on an infinite slope model, and it takes into account the increase in strength and



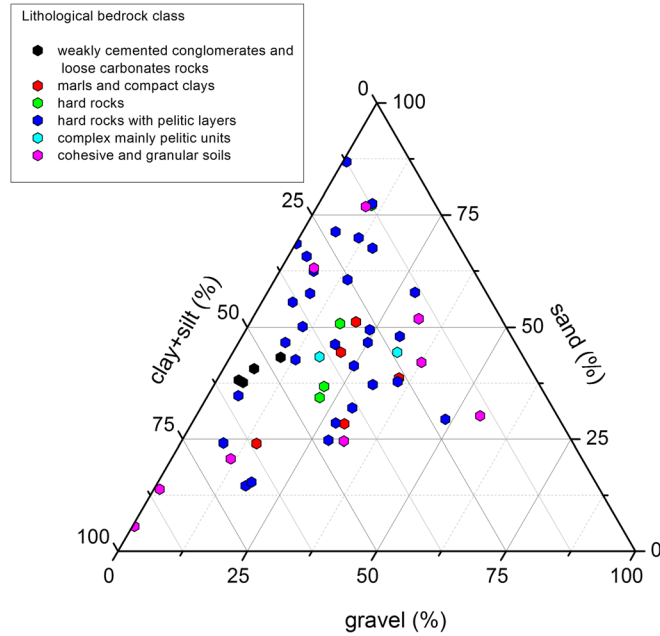


**Fig. 3** Grain size tertiary classification. The 59 survey points are grouped according to the main lithological classes

cohesion due to matric suction in unsaturated soils, where the pressure head is negative. The soil mass variation on partially saturated soil caused by water infiltration is also modeled. The equation of Factor of Safety in unsaturated conditions is (Rossi et al. 2013):

$$FS = \frac{\tan\phi}{\tan\alpha} + \frac{c'}{\gamma_d y \sin\alpha} \frac{\gamma_w h \tan(\phi) \left(1 + \left[\frac{h_b|h|}{\lambda+1}\right]^{\frac{\lambda}{\lambda+1}}\right)^{-1}}{\gamma_d y \sin\alpha}$$

where  $\alpha$  is the slope angle,  $h$  is the pressure head,  $h_b$  is the bubbling pressure, and  $\lambda$  is the pore size index distribution.

In saturated condition, the equation of Factor of Safety is (Rossi et al. 2013):

$$FS = \frac{\tan\phi}{\tan\alpha} + \frac{c'}{[\gamma_d(y-h) + \gamma_{sat}h]\sin\alpha} - \frac{\gamma_w h \tan\phi}{[\gamma_d(y-h) + \gamma_{sat}h]\sin\alpha}$$

where  $\gamma_{sat}$  is the saturated soil unit weight.

For more information on the HIRESSES model, refer to Rossi et al. (2013).

HIRESSES computes the factor of safety at each selected time step (and not only at the end of the rainfall event) and at different depths within the soil layer. In addition to rainfall, the model input data consist of slope gradient, geotechnical and hydrological parameters, and soil thickness (Rossi et al. 2013, Mercogliano et al. 2013). The HIRESSES code can operate at any spatial resolution. Furthermore, in order to manage the problems related to the uncertainties in the main hydrological and mechanical parameters, a Monte Carlo simulation has been implemented.

The input parameters of the model can be divided into two classes: (i) the static data and (ii) the dynamical data. Dynamical

data are the rainfall data. The static data necessary for the model are effective cohesion ( $c'$ ), friction angle ( $\phi'$ ), slope gradient, dry unit weight ( $\gamma_d$ ), soil thickness, hydraulic conductivity ( $k_s$ ), initial soil saturation ( $S$ ), pore size index ( $\lambda$ ), bubbling pressure ( $h_s$ ), effective porosity ( $n$ ), and residual water content ( $\theta_r$ ).

The HIRESSES code has been tested by simulating a past event (24 October 2010–26 October 2010), during which an intense rainstorm affected a part of the study area and it triggered 50 reported shallow landslides. The total precipitation in 3 days was around 250 mm. The hourly rainfall data used for the simulation are the estimated rainfalls derived from the national meteorological radar network, while the static data (geotechnical and hydrological) have been measured in the field and statistically analyzed. The GIST model (Catani et al. 2010) has been applied in the study area in order to get a distributed soil thickness map, while a DTM with a spatial resolution of 10 m has been used to derive the slope gradient. A 10-m cell resolution has been adopted for the model output because it corresponds to the grid size of the Digital Terrain Model (DTM) of the area and because it represents a fair compromise between spatial accuracy and computational resources needed.

## Results

### Geotechnical parameters

In this study, 59 sites were investigated (Fig. 2, Table 1), in the period from June 2014 to December 2014. With respect to the grain size distribution, the materials are quite heterogeneous, as testified by the dispersion in the ternary diagrams Gravel-Sand-Silt + Clay (Fig. 3), being classified as prevalent silty-clayey sand (SM, SC, and SM-SC with respect to the USCS classification; Wagner 1957), with extremely variable gravel fraction (0.2–57.9%) and clay fraction (0.7–42.8%) contents. The dry unit weight ( $\gamma_d$ ) was comprised between 10.4 and 21.3 kN m<sup>-3</sup>. The natural water content was consistently variable (from 4.1 to 43.5% by weight), mainly because the samples were collected both in the wet and

**Table 2** Geotechnical properties of the soil cover of the six lithological classes

Bedrock lithological class of the soil cover	Statistics	$\phi'$ (°)	$c$ (kPa)	$k_v$ (m s <sup>-1</sup> )	Gravel (%)	Sand (%)	Silt (%)	Clay (%)	$w_{cl}$ (%)	$\gamma_d$ (kN m <sup>-3</sup> )	$W_L$ (%)	$W_P$ (%)	IP (%)
Conglomerates and poorly cemented carbonate rocks (5 sites)	Mean	29	6	3,52E-07	7.6	32.6	43.9	15.9	15.2	n.a.	40	33	7
	Median	28	5	3,47E-07	6.8	31.9	42.4	14.5	15.0	n.a.	41	34	7
	Max	34	14	3,47E-07	11.2	35.1	46.7	21.8	24.9	n.a.	42	39	13
	Min	23	2	1,11E-07	4.8	29.7	41.1	12.6	4.1	n.a.	36	23	2
Marls and compact clays (5 sites)	Mean	36	5	5,95E-07	26.4	31.9	29.6	12.1	16.0	16.1	33	22	11
	Median	37	4	5,77E-07	23.3	34.6	27.9	9.1	16.2	15.0	35	23	10
	Max	38	12	8,76E-07	37.3	45.8	44.0	22.0	22.4	21.1	36	31	18
Hard rocks (4 sites)	Mean	32	0	2,62E-07	15.9	18.0	19.0	7.5	9.6	12.3	26	16	5
	Median	32	9	6,89E-07	20.8	44.8	28.6	5.8	33.8	n.a.	47	29	18
	Max	33	11	3,40E-07	21.7	37.5	31.4	9.5	43.5	n.a.	53	29	19
Hard rocks with pelitic layers (33 sites)	Mean	35	12	1,40E-06	24.1	74.9	37.7	10.9	43.5	n.a.	57	37	29
	Median	27	4	3,27E-07	11.4	27.5	12.8	0.8	14.5	n.a.	26	20	6
	Max	33	5	2,57E-06	15.7	42.5	34.7	7.1	21.7	15.5	34	24	10
Complex mainly pelitic units (2 sites)	Mean	34	3	9,78E-07	18.2	39.1	29.7	6.2	21.0	14.5	32	24	7
	Median	42	19	2,70E-05	50.9	85.4	56.7	25.7	43.5	19.4	57	37	33
	Max	20	0	8,20E-08	0.2	10.5	9.1	0.7	4.3	11.4	23	14	3
Cohesive and granular soils (10 sites)	Mean	36	11	7,86E-07	26.4	39.4	25.1	9.2	11.9	n.a.	n.a.	n.a.	n.a.
	Median	36	11	7,86E-07	26.7	38.4	26.0	9.0	11.9	n.a.	n.a.	n.a.	n.a.
	Max	41	13	1,04E-06	34.0	40.5	34.7	9.6	13.9	n.a.	n.a.	n.a.	n.a.
Cohesive and granular soils (10 sites)	Mean	31	9	5,28E-07	19.4	36.3	17.2	8.3	9.9	n.a.	n.a.	n.a.	n.a.
	Median	30	4	7,00E-07	22.0	32.0	31.5	14.0	17.1	11.4	40	26	14
	Max	29	3	4,00E-07	12.0	27.6	31.0	4.3	16.2	11.4	36	30	14
Cohesive and granular soils (10 sites)	Mean	38	10	2,00E-06	57.9	74.4	58.4	42.8	23.5	12.8	58	34	30
	Min	23	0	2,00E-07	0.4	3.7	12.5	0.7	13.4	10.2	25	11	2

n.a. not applicable

**Table 3** HIRESSS input data

Bedrock lithological class	Median grain size	$\phi'$ (°)	$c'$ (kPa)	$k_s$ (m s <sup>-1</sup> )	$\gamma_d$ (kN m <sup>-3</sup> )	Effective porosity (% v/v)	Bubbling pressure	Grain size index	Residual water content
Weakly cemented conglomerates and loose carbonates rocks	Sandy silt	28	0	3,E-07	11.5	41.2	14.66	0.322	0.041
Marls and compact clays	Silty gravelly sand	37	0	6,E-07	15.0	41.7	7.26	0.592	0.020
Hard rocks with pelitic layers	Silty gravelly sand	34	0	1,E-06	14.5	41.7	7.26	0.592	0.020
Cohesive and granular soils	Silty sand	29	0	4,E-07	11.4	40.1	8.69	0.474	0.035

dry season. Also, the bulk porosity ( $n$ ) values span across a wide interval: from 18.2 to 56.3%.

Concerning the Atterberg limits, performed on selected samples, the highest liquid ( $W_L$ ) and plastic ( $W_P$ ) limits, as well as the highest plasticity index (IP), respectively, 58, 39, and 33% by weight, were found on the clay-rich samples (MH and CH in USCS classification). On average, the soils analyzed show a slightly plastic behavior. This is in agreement with the mineralogical composition of these kinds of materials. In fact, in Tuscany, the mineralogical assemblage of hillslope soils consists of quartz, feldspars, plagioclase, and clay minerals with kaolinite predominant over illite and montmorillonite (Masi 2016).

The shear strength parameters obtained in situ are influenced by the saturation degree, inferred by the matric suction measurement. Matric suction values can be divided into two main groups: the first one with values from 1.4 to 5 kPa related to saturated to slightly unsaturated soils

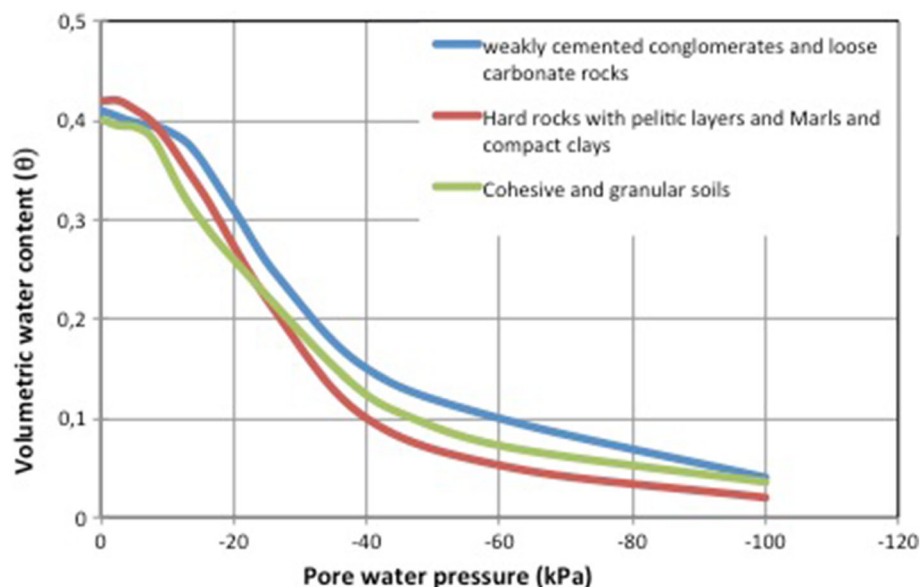
and a second one, from 5 to over 90 kPa, that represents a state of unsaturation (e.g., Fredlund and Rahardjo 1993). The internal friction angle  $\phi'$  measured with BST spanned from 20° to 42°, while the total cohesion ranged from 0 to 19 kPa. The different state of saturation of the investigated sites is the main factor for such a great difference among cohesion values, the higher ones corresponding to unsaturated soils with high matric suction values (up to 90 kPa).

For four survey points, also laboratory direct shear tests (DT) have been carried out (Table 1). For the same site, results of BST and DT are quite similar and comparable (Tofani et al. 2006, Casagli et al. 2006).

The hydraulic conductivity is measured after reaching the saturation of the soils and ranges from  $8 \times 10^{-8}$  to  $3 \times 10^{-5}$  m s<sup>-1</sup>.

#### HIRESSS input data

A step further, the geotechnical properties of the soils have been analyzed with respect to a lithological classification of the

**Fig. 4** Soil characteristic curves for the four soil covers of the main lithologies

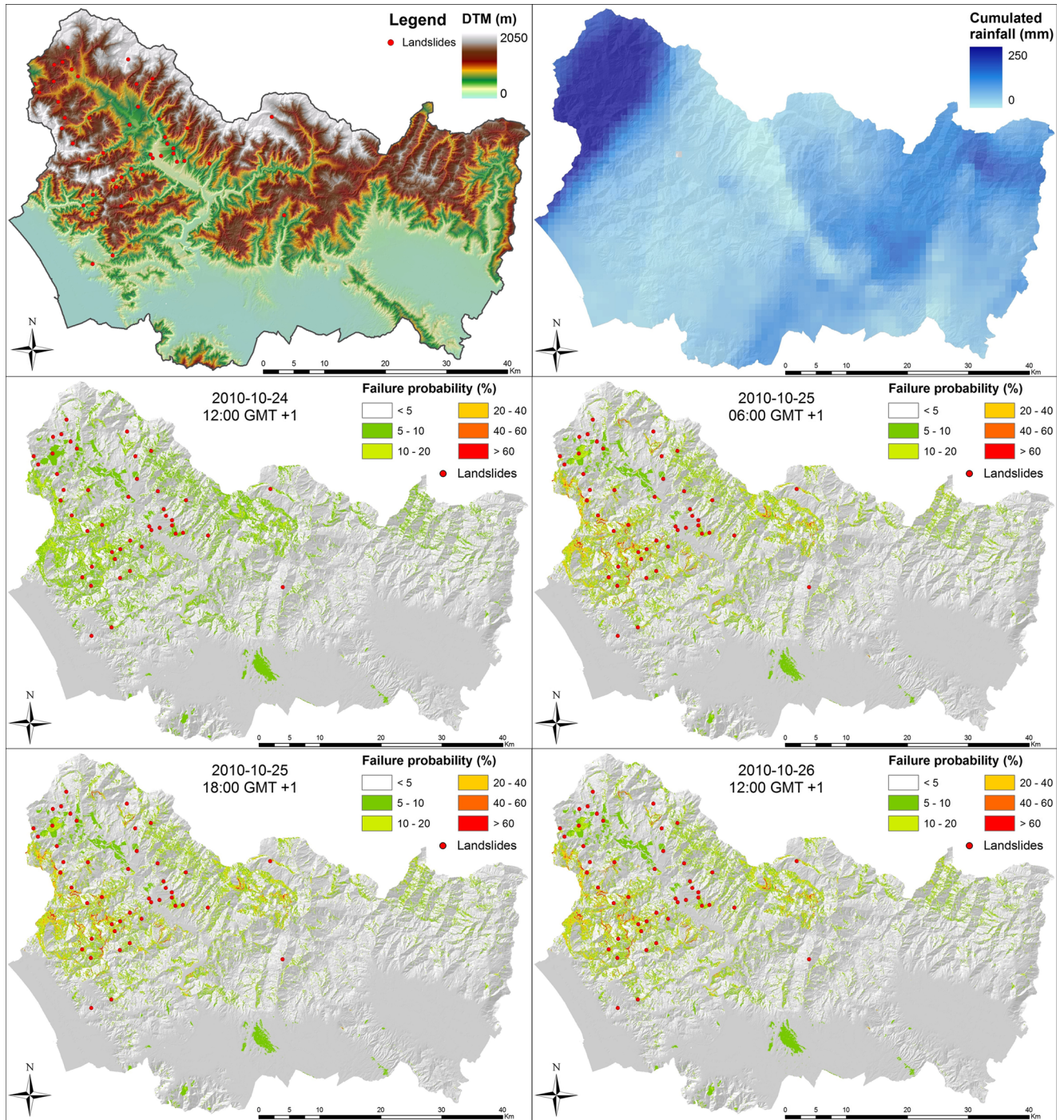


**Fig. 5** Results of HIRESSS simulation. a DTM of the study area with landslides overlapped, b map of the cumulated rainfall during the event, and c-f maps of the probability of instability for four different time steps

underlying bedrock; then for each class of bedrock lithology, the principal parameters of respective soil cover have been resumed (Table 2). Two soil cover classes (those lying over a bedrock classified as “hard rocks” and “complex mainly pelitic units”) have a low density of surveyed points; therefore, their data have been merged to those pertaining to the soil cover of the “rocks with pelitic layers,” which is very similar from a lithological point of view.

Eventually, these data have been employed in order to feed the HIRESSS model. In particular, for the parameters directly measured in the field, the median values have been selected for each lithological class (Table 3). The median was adopted instead of the arithmetic mean, since the latter is not a reliable central tendency parameter because its calculation is strongly affected in some cases by the presence of extremely high or low outlier values. The effective cohesion was set to 0 kPa,



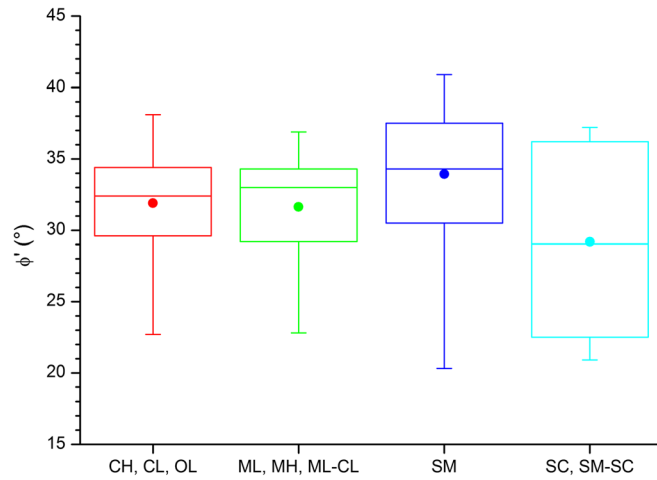


**Fig. 6** Box plot of the friction angle ( $\phi'$ ) classified following the USCS classification

considering that the sampled soils are mostly granular and relatively recent (likely normal consolidated). Finally, the parameters related to the soil water characteristic curve (i.e., bubbling or air entry pressure, grain size index, and residual water content) as well as the effective porosity, which have not been measured, have been derived from Rawls et al. (1982) by matching for each lithological class the corresponding (median) grain size derived from grain size distribution analyses (Table 3). Typical characteristic curves of soil covers have been derived for the main bedrock lithologies on the base of grain size distribution (Fig. 4).

#### HIRESSS simulation

The output of the HIRESSS code is a series of instability maps (one for each time step) where each pixel is associated with a probability of instability. The time step is 1 h. In this simulation, we obtained 72 hourly time steps, covering a timeframe from 24-10-2010 00:00 GMT + 1 to 26-10-2010 24:00 GMT + 1. The simulation results are shown in Fig. 4, where four failure probability maps have been selected as representative of the event. At 12:00 GMT + 1 of 24-10-2010, a generalized situation of stability can be observed in the whole area. At 6:00 GMT + 1 and in the late afternoon (18:00

GMT + 1) of 25-10-2010, the instability conditions increase in the western part of the study area where the failure probability reaches the 60%. In the eastern part of the study area, the failure probability is quite low (around 10%). Of the 26-10-2010, the simulated stability conditions persist critical as the day before, again localized in the western part.

Official reports state that all landslides triggered the 25-10-2016 and the 26-10-2016. The simulation matches quite well with the ground truth observed during this period. The simulated instability conditions start the 25-10-2010 and persist the 26-10-2010. Moreover, the simulation indicates the western part of the study area as the most probable for landslide triggering, followed by the central northern area. The spatial distribution of landslides is partially in accordance with this outcome.

#### Discussion

In this work, we have tried to spatialize (to study the relationship between the values of the data with respect to their spatial distribution) the geotechnical and hydrological input data derived from the performed measurements in order to feed the HIRESSS model with spatially continuous and reliable data (Fig. 5). The parameters have been divided and studied according to the characteristics of the bedrock, which was subdivided into lithological classes.

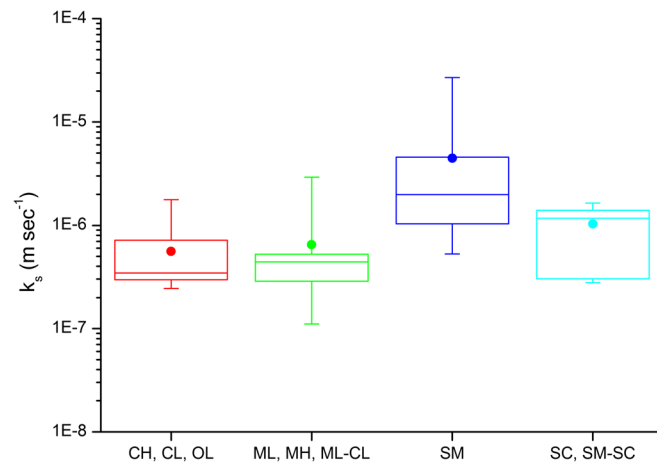


**Fig. 7** Box plot of the saturated permeability ( $k_s$ ) classified following the USCS classification

**Table 4** Extension and density of the survey points of each lithological class

Bedrock lithological class	Extension (%)	Density of survey points (n°/km <sup>2</sup> )
Conglomerates and poorly cemented carbonate rocks	3	0.07
Marls and compact clays	4	0.04
Hard rocks	15	0.01
Hard rocks with pelitic layers	54	0.02
Complex mainly pelitic units	9	0.01
Cohesive and granular soils	15	0.01

As shown in Table 2, all the parameters measured show a relatively high variability for all the lithologies. For example, the range of variation (the difference from the minimum and maximum values) of the effective friction angle ( $\phi'$ ) is very high reaching the value of  $19^\circ$  for the hard rocks with interbedded siltstones. Also, the saturated conductivity ( $k_s$ ) reaches a range of variability of three orders of magnitude for the same lithological class, being still very variable also for all the other classes. Furthermore, the mean and median values are quite similar among the different classes except for the soils (granular and cohesive) and the conglomerates and poorly cemented carbonate rocks.

Figures 6 and 7 show the distribution of  $\phi'$  and  $k_s$  for all the samples on the basis of the USCS classification without taking into account the bedrock lithology. In this case, it is possible to observe a clearer correspondence between the values of the parameters and the grain size distribution of the sample. As it can be expected, the friction angle is higher for the silty sands (SM) than for the clays (CH, CL, OL), silts (ML, MH, ML-CL), and sand-clay mixture (SC, SM-SC). This behavior is even clearer for the  $k_s$  values, with high values of permeability for sandy soils (around values of  $10^{-5} \text{ m s}^{-1}$ ) and medium to low values for clayey silty soils (between  $10^{-6}$  and  $10^{-7} \text{ m s}^{-1}$ ). These results show that the geotechnical and hydrological properties of the soils are mainly related to the soil grain size distribution and suggests on the other hand that a spatialization scheme of the geotechnical and hydrological properties only based on the bedrock lithology (Table 3) is not sufficient to properly characterize the soils.

The lack of correspondence between the soils geotechnical parameters and the underlying bedrock lithology could be due to (i) the insufficient number of survey points for each lithology or to (ii) the effect of other factors controlling the behavior of the parameters. Owing to the first point, the density of the survey points in the whole area and for each lithology is reported in Table 4. The values are quite low especially for some lithologies such as hard rocks, complex mainly pelitic units, and granular and cohesive soils. Granular and cohesive soils mainly outcrop in plain areas, and this is the reason why the survey density is low since the analysis is focused on the soil characterization for landslide occurrence. Instead, for the hard rocks and complex mainly pelitic units, low-density value may result from an incorrect characterizations of the upper soils. Due to this lack of data, in the analysis with HIRESSS, these two classes have been merged with the “hard rocks with pelitic layers” class in order to have more reliable data. Soil characterization will surely benefit from an increase in the number of

survey points for all the lithologies and especially for the lithologies with lower survey density.

Concerning the second point, it is worth noticing that the soil cover (the loose material over the weathered bedrock) is not necessarily derived only by the weathering of the on-site underlying bedrock but also comprised of weathered material that has moved along the slope due to several processes (such as rainwash, sheetwash, and downslope creep). For this reason, further studies can be carried out in order to define a correct approach to spatialize the data so that their behavior could be based not only on the lithology but also on other parameters, such as slope angle, land cover, and especially the effect of the vegetation, soil thickness, and distance from the crest.

The geotechnical and hydrological parameters spatialized have been used to feed the HIRESSS model, simulating a past rainfall event that has triggered in the study area around 50 landslides. The results of the simulation carried out with hourly time-step have been validated with landslides occurred during the event. The validation is only qualitative since a quantitative one is not possible due to the following reasons:

- Actual temporal occurrence (date and hour) of landslides is not available, as the official reports provide only a time frame, from 25 October 2016 to 26 October 2016.
- Landslide inventory is not complete and the lack of reporting is because some portions of the study area are scarcely populated mountainous regions, while most of reported landslides involved infrastructure or water streams.
- A quantitative validation of the results cannot be performed, because it would require the definition of calibration procedures to translate the probabilistic outputs into warning levels.

The visual comparison between the probability of instability maps and the distribution of landslides occurred could allow some general considerations:

- The reported landslide distribution is in general agreement with the probability of instability maps. Landslides are located where the probability of instability is the highest.
- Even though the maximum total rainfall (>200 mm) during 3 days is located in the western and central east part, landslides mainly occurred in the western part. This could mean a strong conditioning by geology and geomorphology and consequently by the soil geotechnical and geomorphological parameters.

In general, the results show that a detailed soil parameter characterization and spatialization could have increased the capacity of the prediction model to correctly identify the areas with the higher landslide instability potential.

Further studies have to be carried out in order to treat soil parameters in a probabilistic way. Further improvements can be obtained considering that the uncertainty associated to some parameters such as friction angle or hydraulic conductivity can be evaluated by using a normal Gaussian frequency model (Bicocchi et al. 2016). The advantage of adopting a normal distribution model is double: The uncertainty associated with the input parameters is more realistic than using an equiprobable one. Indeed, given a mean value and a standard deviation obtained from the samples analyzed, extremely low or high values are associated to low probability of occurrence, dramatically reducing the simulation time. These upgrades are expected to positively affect the efficiency of the numerical model allowing us to perform simulations on larger time scale, so that the assessment of slope stability and landslides triggering mechanisms will improve (Bicocchi et al. 2016).

### Conclusions

In this work, we report some preliminary results of the IPL project no. 198 “Multi-scale rainfall triggering models for Early Warning of Landslides (MUSE).”

In a 3103-km<sup>2</sup> test area, located in northern Tuscany (Italy), we have carried out a detailed geotechnical characterization of the soil cover through in situ and laboratory tests in 59 survey points. The results have been statistically treated, and they have been spatialized according to the main lithologies in the area. These data have been then used to feed a physically based model, the HIRESSS, for the prediction of shallow landslides. A past event has been selected to back-analyze the capability of the model, fed with detailed geotechnical and hydrological parameters, to predict the landslide occurrence at regional scale. This event, occurred in October 2010, has triggered around 50 landslides in the study area.

The qualitative validation has shown that a detailed soil parameter characterization and spatialization may increase the capacity of the prediction model to correctly identify the areas with highest instability potential during the rainfall event. The use of real data collected in the field as input for HIRESSS model is expected to provide better results than the use of literature data in terms of slope instability mechanism prevision.

Some further analyses need to be carried out in order to define a correct approach to spatialize the data that can be based not only on the lithology but also on other parameters, such as slope angle, land cover, and especially the effect of the vegetation, soil thickness, and distance from the crest. The same improvements have to be carried out in order to introduce the soil parameters uncertainties using normal Gaussian frequency model. The final aim is to define a standard and reproducible procedure to spatialize the input geotechnical and hydrological data of the landslide prediction models in order to increase their capability to deal with real-time landslide prediction.

### Acknowledgements

This research has been performed in the framework of the IPL project no. 198. The authors are grateful to Dr. Pietro Vannocci and Dr. Carlo Tacconi Stefanelli for their support during field and laboratory tests.

**Open Access** This article is distributed under the terms of the Creative Commons Attribution 4.0 International License (<http://creativecommons.org/licenses/by/4.0/>), which permits unrestricted use, distribution, and reproduction in any medium, provided you give appropriate credit to the original author(s) and the source, provide a link to the Creative Commons license, and indicate if changes were made.

### References

- Amoozegar A (1989) Compact constant head permeameter for measuring saturated hydraulic conductivity of the vadose zone. *Soil Sci Soc Am J* 53:1356–1361
- Arnone E, Noto L, Lepore C, Bras R (2011) Physically-based and distributed approach to analyze rainfall-triggered landslides at watershed scale. *Geomorphology* 133:121–131 2011
- Baroni G, Facchi A, Gandolfi C, Ortuani B, Horeschi D, van Dam JC (2010) Uncertainty in the determination of soil hydraulic parameters and its influence on the performance of two hydrological models of different complexity *Hydrological Earth Syst Sci* 14:251–270
- Baum R, Savage W, Godt J (2002) Trigs: A fortran program for transient rainfall infiltration and gridbased regional slopestability analysis. Open-file Report, US Geological Survey, 2002
- Baum RL, Godt JW, Savage WZ (2010) Estimating the timing and location of shallow rainfall-induced landslides using a model for transient unsaturated infiltration. *J Geophys Res* 115:F03013
- Bicocchi G, D'Ambrosio M, Rossi G, A. Rosi, Tacconi-Stefanelli C, Segoni S, Nocentini M, Vannocci P, Tofani V, Casagli N, Catani F, (2016) Shear strength and permeability in situ measures to improve landslide forecasting models: a case study in the Eastern Tuscany (Central Italy). In book: Landslides and engineered slopes. Experience, Theory and Practice, 419–424, DOI: [10.1201/b21520-42](https://doi.org/10.1201/b21520-42)
- Carrara A, Crosta G, Frattini P (2008) Comparing models of debris-flow susceptibility in the alpine environment. *Geomorphology* 94:353–378
- Casagli N, Dapporto S, Ibsen ML, Tofani V, Vannocci P (2006) Analysis of the landslide triggering mechanism during the storm of 20th–21th November 2000, in northern Tuscany. *Landslides* 3:13–21
- Catani F, Casagli N, Ermini L, Righini G, Menduni G (2005) Landslide hazard and risk mapping at catchment scale in the Arno River basin. *Landslides* 2(4):329–342
- Catani F., Segoni S., Falorni G. (2010) An empirical geomorphology-based approach to the spatial prediction of soil thickness at catchment scale. *Water Resources Research*, 46 (5)
- Chen HX, Zhang LM (2014) A physically-based distributed cell model for predicting regional rainfall-induced shallow slope failures. *Engineering Geology* doi: [10.1016/j.enggeo.2014.04.011](https://doi.org/10.1016/j.enggeo.2014.04.011)
- D'Amato Avanzi G, Falaschi F, Giannecchini R, Puccinelli A (2009) Soil slip susceptibility assessment using mechanical–hydrological approach and GIS techniques: an application in the Apuan alps (Italy). *Nat Hazards* 50(3):591–603
- D'Amato Avanzi G, Galanti Y, Giannecchini R, Lo PD, Puccinelli A (2013) Estimation of soil properties of shallow landslide source areas by dynamic penetration tests: first outcomes from northern Tuscany (Italy). *Bull Eng Geol Environ* 72(3):609–624
- Dietrich W, Montgomery D (1998) Shalstab: a digital terrain model for mapping shallow landslide potential. NCASI (National Council for Air and Stream Improvement) Technical Report, February, 1998
- Dirksen C (1999) Soil physics measurements. Catena Verlag, pp.154
- Fredlund DG, Rahardjo H (1993) Soil mechanics for unsaturated soils. John Wiley & Sons, New York
- Fredlund DG, Morgenstern NR, Widger RA (1978) The shear strength of unsaturated soils. *Can Geotech J* 15:312–321
- Giannecchini R (2006) Relationship between rainfall and shallow landslides in the southern Apuan alps (Italy). *Nat Hazards Earth Syst Sci* 6:357–364. doi:[10.5194/nhess-6-357-2006](https://doi.org/10.5194/nhess-6-357-2006) 2006
- Giannecchini R, Naldini D, D'Amato Avanzi G, Puccinelli A (2007) Modelling of the initiation of rainfall-induced debris flows in the Cardoso basin (Apuan Alps, Italy). *Quaternary International*, Volumes 171–172, August–September 2007, Pages 108–117
- Griffiths DV, Huang JS, Fenton GA (2011) Probabilistic infinite slope analysis. *Comput Geotech* 38(4):577–584
- Jia N, Mitani Y, Xie M, Djameluddin I (2012) Shallow landslide hazard assessment using a three-dimensional deterministic model in a mountainous area. *Comput Geotech* 45(2012):1–10
- Jiang SH, Li DQ, Zhang LM, Zhou CB (2013) Slope reliability analysis considering spatially variable shear strength parameters using a non-intrusive stochastic finite element method. *Eng Geol* 168:120–128

- Lepore C, Arnone E, Noto LV, Sivandran G, Bras RL (2013) Physically based modeling of rainfall-triggered landslides: a case study in the Luquillo forest. *Puerto Rico Hydrol Earth Syst Sci* 17:3371–3387
- Lu N, Godt J (2008) Infinite slope stability under steady unsaturated seepage conditions. *Water Resour Res* 44:11
- Lutenegger AJ, Halberg GR (1981) Borehole shear test in geotechnical investigation. *Special technical Publ. Am Soc Test Mater* 740:566–578
- Mallants D, Jacques D, Tseng PH, van Genuchten MT, Feyena J (1997) Comparison of three hydraulic property measurement methods. *J Hydrol* 199:295–318
- Masi, E.B. (2016) Determination of the organic matter content in some soils of Tuscany and correlation with their geotechnical and mineralogical properties. MSc dissertation, University of Florence, 97 pp
- McKenzie N, Cresswell H (2008) Selecting a method for hydraulic conductivity. In: McKenzie N, Coughlan K, Cresswell H (eds) *Soil physical measurement and interpretation for land evaluation*. SBS Publishers & Distributors PVT. Ltd., New Delhi, pp 90–107
- Mercogliano P, Segoni S, Rossi G, Sikorsky B, Tofani V, Schiano P, Catani F, Casagli N (2013) Brief communication: a prototype forecasting chain for rainfall induced shallow landslides. *Nat Hazards Earth Syst Sci* 13:771–777
- Montrasio L, Valentino R, Losi GL (2011) Towards a real-time susceptibility assessment of rainfall-induced shallow landslides on a regional scale. *Nat Hazards Earth Syst Sci* 11:1927–1947 2011
- Pack R, Tarboton D, Goodwin C (2001) Assessing terrain stability in a GIS using SINMAP, in: 15th Annual GIS Conference, GIS, 2001
- Park HJ, Lee JH, Woo I (2013) Assessment of rainfall-induced shallow landslide susceptibility using a GIS-based probabilistic approach. *Eng Geol* 161:1–15
- Philip JR (1985) Approximate analysis of the borehole permeameter in unsaturated soil. *Water Res Res* 21:1025–1033
- Rawls WJ, Brakensiek DL, Saxton KE (1982) Estimation of soil water properties. *Trans ASAE* 25:1316–1320
- Ren D, Fu R, Leslie LM, Dickinson R, Xin X (2010) A storm-triggered landslide monitoring and prediction system: formulation and case study. *Earth Interact* 14:1–24
- Ren D, Leslie L, Lynch M (2014) Trends in storm-triggered landslides over Southern California. *J Appl Meteor Climatol* 53:217–233
- Rinaldi M, Casagli N (1999) Stability of streambanks formed in partially saturated soils and effects of negative pore water pressures: the Sieve River (Italy). *Geomorphology* 26:253–277
- Rossi G, Catani F, Leoni L, Segoni S, Tofani V (2013) HIRESSS: a physically based slope stability simulator for HPC applications. *Nat Hazards Earth Syst Sci* 13:151–166 2013
- Santoso AM, Phoon KK, Quek ST (2011) Effects of soil spatial variability on rainfall induced landslides. *Comput Struct* 89:893–900
- Segoni S, Leoni L, Benedetti AI, Catani F, Righini G, Falorni G, Gabellani S, Rudari R, Silvestro F, Rebori N (2009) Towards a definition of a real-time forecasting network for rainfall induced shallow landslides. *Nat Hazards Earth Syst Sci* 9:2119–2133
- Simoni S, Zanotti F, Bertoldi G, Rigon R (2008) Modelling the probability of occurrence of shallow landslides and channelized debris flows using geotop-fs. *Hydrol Process* 22:532–545
- Tao J, Barros AP (2014) Coupled prediction of flood response and debris flow initiation during warm- and cold-season events in the southern Appalachians. *USA Hydrol Earth Syst Sci* 18:367–388 2014
- Tofani V, Dapporto S, Vannocci P, Casagli N (2006) Infiltration, seepage and slope instability mechanisms during the 20–21 November 2000 rainstorm in Tuscany, Central Italy. *Nat Hazards Earth Syst Sci* 6:1025–1033
- Vai GB, Martini IP (2001) *Anatomy of an Orogen: the Apennines and adjacent Mediterranean basins*. Kluwer Acad. Publ, Dordrecht 633 p
- Wagner AA (1957) *The use of the Unified Soil Classification System by the Bureau of Reclamation*. Proceedings of the 4th International Conference on Soil Mechanics and Foundation Engineering: I: 125, London
- Warrick AW, Nielsen DR (1980) Spatial variability for soil physical properties in the field. In: Hillel D (ed) *Applications of soil physics*. Academic Press, Toronto, pp 319–344
- Zizioli D, Meisina C, Valentino R, Montrasio L (2013) Comparison between different approaches to modeling shallow landslide susceptibility: a case history in Oltrepò Pavese. Northern Italy *Nat Hazards Earth Syst Sci* 13:559–573 2013

V. Tofani (✉) · G. Biccocchi · G. Rossi · S. Segoni · M. D'Ambrosio · N. Casagli · F. Catani

Department of Earth Sciences,  
University of Firenze,  
Via G. La Pira 4, 50121, Florence, Italy  
e-mail: veronica.tofani@unifi.it